Bull Volcanol (1999) 61:306–323

ORIGINAL PAPER

K. V. Cashman · C. Thornber · J. P. Kauahikaua

Cooling and crystallization of lava in open channels, and the transition of Pāhoehoe Lava to ʻAʻā

Received: 3 September 1998 / Accepted: 12 April 1999

Abstract Samples collected from a lava channel active at Kīlauea Volcano during May 1997 are used to constrain rates of lava cooling and crystallization during early stages of flow. Lava erupted at near-liquidus temperatures (~1150 °C) cooled and crystallized rapidly in upper parts of the channel. Glass geothermometry indicates cooling by 12–14 °C over the first 2 km of transport. At flow velocities of 1–2 m/s, this translates to cooling rates of 22–50 °C/h. Cooling rates this high can be explained by radiative cooling of a well-stirred flow, consistent with observations of non-steady flow in proximal regions of the channel. Crystallization of plagioclase and pyroxene microlites occurred in response to cooling, with crystallization rates of 20–50% per hour. Crystallization proceeded primarily by nucleation of new crystals, and nucleation rates of ~10^4/cm^3s are similar to those measured in the 1984 open channel flow from Mauna Loa Volcano. There is no evidence for the large nucleation delays commonly assumed for plagioclase crystallization in basaltic melts, possibly a reflection of enhanced nucleation due to stirring of the flow. The transition of the flow surface morphology from pāhoehoe to ʻaʻā occurred at a distance of 1.9 km from the vent. At this point, the flow was thermally stratified, with an interior temperature of ~1137 °C and crystallinity of ~15%, and a flow surface temperature of ~1100 °C and crystallinity of ~45%. ʻAʻā formation initiated along channel margins, where crust was continuously disrupted, and involved tearing and clotting of the flow surface. Both observations suggest that the transition involved crossing of a rheological threshold. We suggest this threshold to be the development of a lava yield strength sufficient to prevent viscous flow of lava at the channel margin. We use this concept to propose that ʻaʻā formation in open channels requires both sufficiently high strain rates for continued disruption of surface crusts and sufficient groundmass crystallinity to generate a yield strength equivalent to the imposed stress. In Hawaiʻi, where lava is typically microlite poor on eruption, these combined requirements help to explain two common observations on ʻaʻā formation: (a) ʻaʻā flow fields are generated when effusion rates are high (thus promoting crustal disruption); and (b) under most eruption conditions, lava issues from the vent as pāhoehoe and changes to ʻaʻā only after flowing some distance, thus permitting sufficient crystallization.

Key words Kīlauea · Basalt crystallization · pāhoehoe · ʻaʻā · Rheology · Lava flow morphology

Editorial responsibility: M. Carroll

Katharine V. Cashman (✉)
Department of Geological Sciences, University of Oregon, Eugene, OR 97405, USA
e-mail: cashman@oregon.uoregon.edu
Tel.: +541-3464323
Fax: +541-3464692

Carl Thornber · James P. Kauahikaua
U.S.G.S. Hawaiian Volcano Observatory, Hawaiʻi National Park, HI 96718, USA

Introduction

Basaltic lava flows are emplaced under a wide range of conditions, yet, as noted by early observers of active lava flows in both Italy (e.g., Scrope 1856; Gemmellaro 1858) and Hawaiʻi (e.g., Dana 1849; Alexander 1859), they can be categorized as one of three lava types: pāhoehoe, ʻaʻā, or blocky. The words "pāhoehoe" and "ʻaʻā" are adopted from the Hawaiian language and first appeared in the scientific literature in Dana's (1849) U.S. Exploring Expedition report (Wright and Takahashi 1989, 1998). Numerous observations and hypotheses about the origin of these two lava types filled the literature for the subsequent century, but it was not until Macdonald's (1953) summary paper that an explicit link was made between flow surface morphology and the mechanism of flow emplacement. The past 20 years have seen increasing attempts to link processes of basaltic lava flow advance, cooling, and crystalliza-

tion to development of flow surface morphology for improved prediction of lava flow behavior during effusive eruptions (e.g., Swanson 1973; Pinkerton and Sparks 1976; Peterson and Tilling 1980; Kilburn 1981, 1990, 1993, 1996; Lipman and Banks 1987; Fink and Griffiths 1990, 1992; Rowland and Walker 1990; Griffiths and Fink 1992a, 1992b, 1993; Crisp et al. 1994; Gregg and Fink 1995).

Basaltic lava flow fields may be classified as either pāhoehoe or ʻaʻā based on the dominant flow morphology. Pāhoehoe flow fields are fed by robust tube systems that allow lava transport over long distances with very little cooling (e.g., Swanson 1973; Greeley 1987; Cashman et al. 1994; Peterson et al. 1994; Helz et al. 1995; Keszthelyi 1995; Kauahikaua et al. 1998). Pāhoehoe flows advance initially as thin sheets or lobes, surface crusts form rapidly, and flows may subsequently inflate if slopes are sufficiently low (Hon et al. 1994). Flow interiors cool by conduction through the enclosing crust, and solidified flow textures are correspondingly finer grained at flow surfaces than in flow interiors (Katz 1997). Vesicles are commonly spherical, and their concentration in the upper parts of flows (e.g., Macdonald 1953; Aubele et al. 1988) reflects extensive syn-emplacement crustal growth accompanying flow inflation (Cashman and Kauahikaua 1997). In contrast, ʻaʻā flow fields form where lava is transported through open channels, most common when eruption rates are high (Macdonald 1953; Pinkerton and Sparks 1976; Rowland and Walker 1990). Channel geometries evolve down flow from narrow and leveed in proximal regions to wide and non-leveed near the thickened flow front (Lipman and Banks 1987; Kilburn and Guest 1993). Flow surfaces change from smooth to rough with increasing distance of transport (e.g., Wolfe et al. 1988; Kilburn 1990), and flow fronts are thick and advance steadily (Kilburn 1993). Solidified flows are aphanitic, and textures are uniform throughout thick flows (Macdonald 1953; Katz 1997). Vesicles, where present, are highly deformed (Polacci and Papale 1997; Polacci et al. 1999), and re-entrained crust is common near upper flow surfaces (Crisp and Baloga 1994).

Morphologic and dynamic differences between lava flow types can be related to variations in the rheology of flow interiors and the strength and thickness of surface crusts. ʻAʻā crusts are weak and fail continuously, whereas pāhoehoe crusts are relatively strong and fail episodically (Kilburn 1990, 1993). The smooth surfaces and thin initiation of pāhoehoe flows suggest that fluid flow cores have Newtonian rheologies (e.g., Hon et al. 1994), and the greater thickness of ʻaʻā flows suggests flow interiors that possess a substantial yield strength (e.g., Robson 1967; Walker 1967; Hulme 1974). Predicting changes in both lava rheology and crustal thickness during flow emplacement is thus critical to accurate modeling of lava flow behavior (e.g., Dragoni 1989, 1993; Dragoni and Tallarico 1994; Miyamoto and Sasaki 1998). Differences in both the mechanical behavior of flow crusts and the rheological behavior of flow interiors reflect contrasting histories of flow cooling and crystallization during emplacement. Consequently, elucidation of the specific conditions under which pāhoehoe transforms to ʻaʻā should improve our general understanding of the parameters controlling lava flow emplacement.

Herein we review the history of field-based observations on the pāhoehoe-ʻaʻā transition as a framework for interpreting new data on lava cooling and crystallization across the transition in a small open channel flow from Kīlauea Volcano, Hawaiʻi.

Early qualitative observations of the pāhoehoe-ʻaʻā transition

Early observations of pāhoehoe and ʻaʻā flow emplacement in Hawaiʻi are summarized in an annotated bibliography of Hawaiian volcanology (Wright and Takahashi 1989). As early as 1849, Dana recognized that both flow surface morphologies could be produced during a single eruptive episode. He interpreted ʻaʻā formation to be a consequence of solidification and subsequent crustal breakage at the flow front and later hypothesized that the size of ʻaʻā clinkers reflected the thickness of cooled crust at the time of their formation (Dana 1888). Alexander's (1859) interpretation of the pāhoehoe-ʻaʻā transition went a step further, because he differentiated the "complete fusion" of pāhoehoe streams from the "less fluid" nature of ʻaʻā, "being full of solid points, or centers of cooling ... [and thus] the aa stream grains like sugar." By the end of the century, observers had documented that the transition was related to the slope over which the lava flowed (Alexander 1886) and was independent of chemical composition (Dutton 1884; Dana 1888). ʻAʻā flows were observed to move with a cooled surface carried over a molten core (Oleson 1880) and to be thicker than pāhoehoe flows. These physical features were attributed to more extensive gas loss (Jaggar 1920) and higher viscosity (Daly 1911; Emerson 1926) of the ʻaʻā. Lava crystallinity was recognized as the primary physical difference between the two flow types (Washington 1923), and dynamic crystallization experiments (Emerson 1926) suggested that stirring, in addition to simple cooling, might explain the high rates of crystallization observed in ʻaʻā (e.g., Finch 1926; Chang 1930; Jaggar 1930). The combination of gas loss and melt crystallization was seen to be consistent with the observed irreversibility of the transition (Stearns and Clark 1930).

Recent quantification of the pāhoehoe-ʻaʻā transition

Modern views of pāhoehoe and ʻaʻā start with Macdonald's (1953) classic paper. Macdonald observed that ʻaʻā flows are common early in eruptive sequences when eruption rates are high, whereas long duration, low-effusion-rate eruptions produce pāhoehoe flow fields. He viewed the transition from pāhoehoe to ʻaʻā to be con-

trolled by viscosity increases resulting from flow cooling, gas loss and crystallization, and suggested the transition to represent a critical relationship between flow viscosity and the amount of "internal disturbance" resulting from flow.

Recent observations of active flows at Kīlauea and Mauna Loa, Hawai'i, and Mt. Etna, Sicily, have provided new qualitative and quantitative data on the transition of pāhoehoe to 'a'ā (e.g., Swanson 1973; Pinkerton and Sparks 1976, 1978; Peterson and Tilling 1980; Kilburn 1981, 1990, 1993; Guest et al. 1987; Lipman and Banks 1987; Rowland and Walker 1987, 1990; Wolfe et al. 1988; Kilburn and Guest 1993; Jurado-Chichay and Rowland 1995; Calvari and Pinkerton 1998). Under conditions of open-channel flow, stable channels develop as fluid lava is focused between confining levees and gradually transforms into 'a'ā through a sequence of textural changes. *Slabby* pāhoehoe forms when smooth crust from the central channel is broken into plates that collide and are disrupted on the flow surface. Farther down channel, clots of spinose lava form at flow margins and aggregate to create a crust of *spinose* (cauliflower) 'a'ā clinkers. With increasing transport distance, the clinkers round as they grind against one another during flow. Transitional surface morphologies, such as pasty pāhoehoe, typify small breakouts from 'a'ā channels, particularly on low-gradient slopes.

What conditions determine the style of lava flow field emplacement? Pinkerton and Sparks (1976) first defined physical conditions leading to generation of a specific flow type with their observations that channelized 'a'ā flows were common at Mt. Etna only for effusion rates in excess of 2×10^{-3} m^3/s. A much higher average effusion rate is apparently required for formation of 'a'ā flows in Hawai'i ($\sim$5–10 m^3/s; Rowland and Walker 1990), most likely a consequence of both shallower slopes and lower initial viscosities of Hawaiian lava (Kilburn 1993). A theoretical framework for the pāhoehoe-to-'a'ā transition was provided by Peterson and Tilling (1980), who formalized Macdonald's (1953) observations by describing the transition as an exceeded threshold in shear strain rate–viscosity space (Fig. 1). This threshold has been interpreted as a failure envelope for flow crusts under conditions of continuous deformation (Kilburn 1990), although the transition also appears to be accompanied by an increase in the effective viscosity of flow interiors due to increasing flow crystallinity (Swanson 1973; Crisp et al. 1994). Rates of crystallization are enhanced by stirring, as shown by recent experimental data (Kouchi et al. 1986; Sato 1995), confirming Emerson's (1926) original hypothesis. Crystallinity increases will also change the rheology of lava through development of yield strength (Sparks and Pinkerton 1978). All of these factors probably play a role in the pāhoehoe-'a'ā transition, but the most widely accepted model remains one of a threshold in viscosity–strain rate space.

Finally, an emerging body of work on the more general topic of flow surface morphology provides a framework for linking the dynamics of flow to flow cooling. These studies show that many aspects of flow morphology can be predicted by a single dimensionless parameter Ψ, which represents the relative importance of quenching (τ_s) and advection (τ_a) time scales (Fink and Griffiths 1990, 1992; Griffiths and Fink 1993). For laminar flow conditions, Ψ represents the distance (measured in flow depths) a flow travels prior to surface crust formation ($\sim 10^2$ s; equivalent to the chilling time scale of Kilburn 1993, 1996). In wax experiments, low Ψ values, where the rates of crust formation are high relative to rates of flow advance, produce lobate flows with flow front advance modulated by pressure build-up and crustal rupture. In contrast, high Ψ values, where advection is much more rapid than crust formation, produce fluid flows with solid crust confined to the vicinity of the flow front. While useful for interpretation of flow morphologies in planetary and submarine environments (Griffiths and Fink 1992a, 1992b), the direct application of Ψ to terrestrial flows is limited by the laminar flow constraint, because open-channel flows, although not strictly turbulent, are commonly well stirred. Any realistic definition of Ψ must also include effects of slope (Gregg and Fink 1995) and yield strength (Griffiths and Fink 1997; Fink and Griffiths 1998).

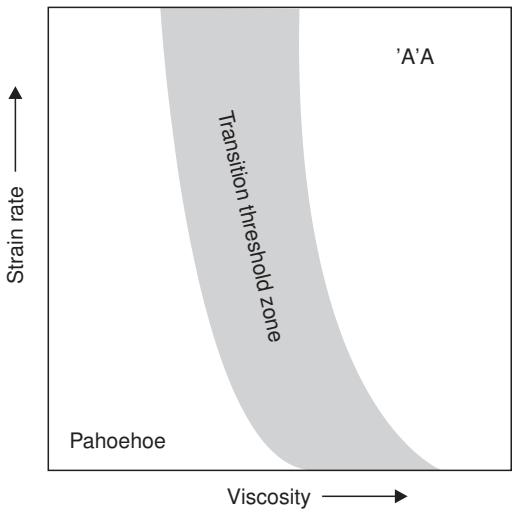

Fig. 1 Diagram of commonly accepted viscosity-strain rate diagram illustrating the conversion of pāhoehoe to 'a'ā. (Modified from Peterson and Tilling 1980)

Questions remaining

Despite the proposed link between crystallization and the transition to 'a'ā, surprisingly few data exist on rates of cooling and crystallization during lava flow under different transport conditions. Also lacking are flow velocity profiles and depth measurements necessary for down-flow strain rate estimates, with the exception of the 1984 lava flow from Mauna Loa (e.g., Lipman and Banks 1987; Moore 1987; Crisp et al. 1994;

Crisp and Baloga 1994). Finally, lava crystallinity–rheology relations are poorly defined. All of these parameters must be constrained for application of thermal models (Crisp and Baloga 1994) and scaling relations (Griffiths and Fink 1993) to predictions of rates and styles of flow advance. Moreover, although it is generally agreed that cooling, crystallization, and consequent increases in viscosity are necessary to produce ʻaʻā, no attempts have been made to quantify the critical viscosity–strain rate threshold hypothesized by Peterson and Tilling (1980). Here we combine analyses of quenched lava textures and glass compositions with flow velocity and channel depth measurements of a single channelized flow, active at Kīlauea Volcano in May 1997, to determine rates of cooling, crystallization, and changes in surface morphology in the proximal regions of this particular lava channel. We then place these observational data in the larger context of conditions required for ʻaʻā formation.

Sample collection and measurement methods

The 1997 activity at Kīilauea Volcano

Favorable patterns of eruptive activity at Kīlauea Volcano during the spring of 1997 afforded an unusual opportunity for sampling an active ʻaʻā channel. At the end of January 1997, after 4 years of relatively stable eruptive conditions, the 15-year-long Puʻu ʻŌʻō Kūpaianaha eruption entered a new stage of activity (Thornber et al. 1997). The 1993 through 1996 eruptive interval (episode 53) was characterized by steady effusion from a vent on the west flank of the Puʻu ʻŌʻō cone, effusion that transported lava to the coast through an 11-km-long tube system (Fig. 2a). On 29 January lava feeding the Puʻu ʻŌʻō vent area was diverted abruptly to an intrusion up-rift, culminating in a fissure eruption in Napau Crater (episode 54). After a month-long hiatus, lava reappeared in the Puʻu ʻŌʻō crater (onset of episode 55), and by late March new vents on the west and southwest flanks of Puʻu ʻŌʻō began to issue lava. During April and May of 1997, lava effusion alternated among four flank vents. Numerous flows from these vents traveled 1–4 km, with further advance prevented by interruptions in lava input to the system. All flows had pāhoehoe morphologies near the vent and flow fronts of ʻaʻā morphology. In the time period leading up to our sampling date, eruptive pauses occurred on 10, 11, 12, and 14 May, and lasted from 5 to 8 h. New lava flows issued from Puʻu ʻŌʻō flank vents after each pause (Fig. 2b). Integrated flow volumes suggest that average effusion rates over this time period were $\sim 3\ m^3/s$. These effusion rates are similar to those of ʻaʻā flows that formed from tube breakouts during the eruption of Mauna Ulu, Kīlauea Volcano (Swanson 1973), although slightly below the minimum rates commonly assumed necessary for ʻaʻā formation (e.g., Rowland and Walker 1990).

The 15–16 May flow (Fig. 2b) began after the 14 May pause and contained the 16 May flow channel that we sampled. This flow was fed sporadically during a slow restart on 14 May, and extended less than 1 km from the vent by the afternoon of the 15 May. An increase in eruptive vigor late in the day produced a channelized ʻaʻā flow that traveled 4 km from the vent. By the morning of 16 May this flow had stagnated at its terminus, and a second channelized flow (the 16 May flow) from the same vent had advanced nearly 3 km along the eastern margin of the 15 May flow. The 16 May flow channel was typically 5–10 m wide with broad (50 m) outer ʻaʻā levees and inner levees of thin pāhoehoe spillovers. On the basis of later measurements of drained channels, we estimate that the channel depth during emplacement was no more than 3 m. Lava flowed through the channel at a velocity of 1–2 m/s and was generally laminar (Reynolds numbers ~50–80). In proximal areas, incipient crust was efficiently recycled by rotational flow through sinuous channels and at the base of small lava falls (e.g., Kauahikaua et al. 1998) and by mechanical mixing as large blocks spalled off channel walls. Channel overflows were most common within 1 km of the vent region, where they produced flows of smooth pāhoehoe. Breakouts from under ʻaʻā crusts in more distal portions of the channel had surfaces with slabby (transitional) pāhoehoe morphologies.

Sample collection, 16 May 1997

Lava from the 16 May channel was sampled from ~1 km of its 4 km extent. Sample locations are shown in Fig. 2b and summarized in Table 1. Sampling of the active channel was complicated by unstable marginal levees, channel overflows, and breakouts and was limited to three locations (1.7, 1.8, and 1.9 km from the vent) that spanned the surface transition from pāhoehoe to ʻaʻā. The first two channel samples (KE55–1885 and 1886) were recovered from stretches of the active channel with smooth, thin, discontinuous surface crusts. To collect samples, we used a steel hammer head suspended in the channel by a cable. This technique allowed sampling through ~1 m of the flow, and samples are representative of the flow interior. Samples KE55–1885 and KE55–1886 were collected, respectively, from above and below a small (~5 m high) lava falls. There was no apparent change in flow surface texture resulting from the elevation drop, indicating that this break in slope alone was insufficient to convert the channelized pāhoehoe to ʻaʻā. Sample KE55–1888 was retrieved by a hammer dipped into the active channel margin just below the point where the flow surface developed a spinose ʻaʻā morphology. This sample is representative of the ʻaʻā surface, not of the flow interior.

The sample suite was extended through limited hammer-dip sampling of active overflows and break-

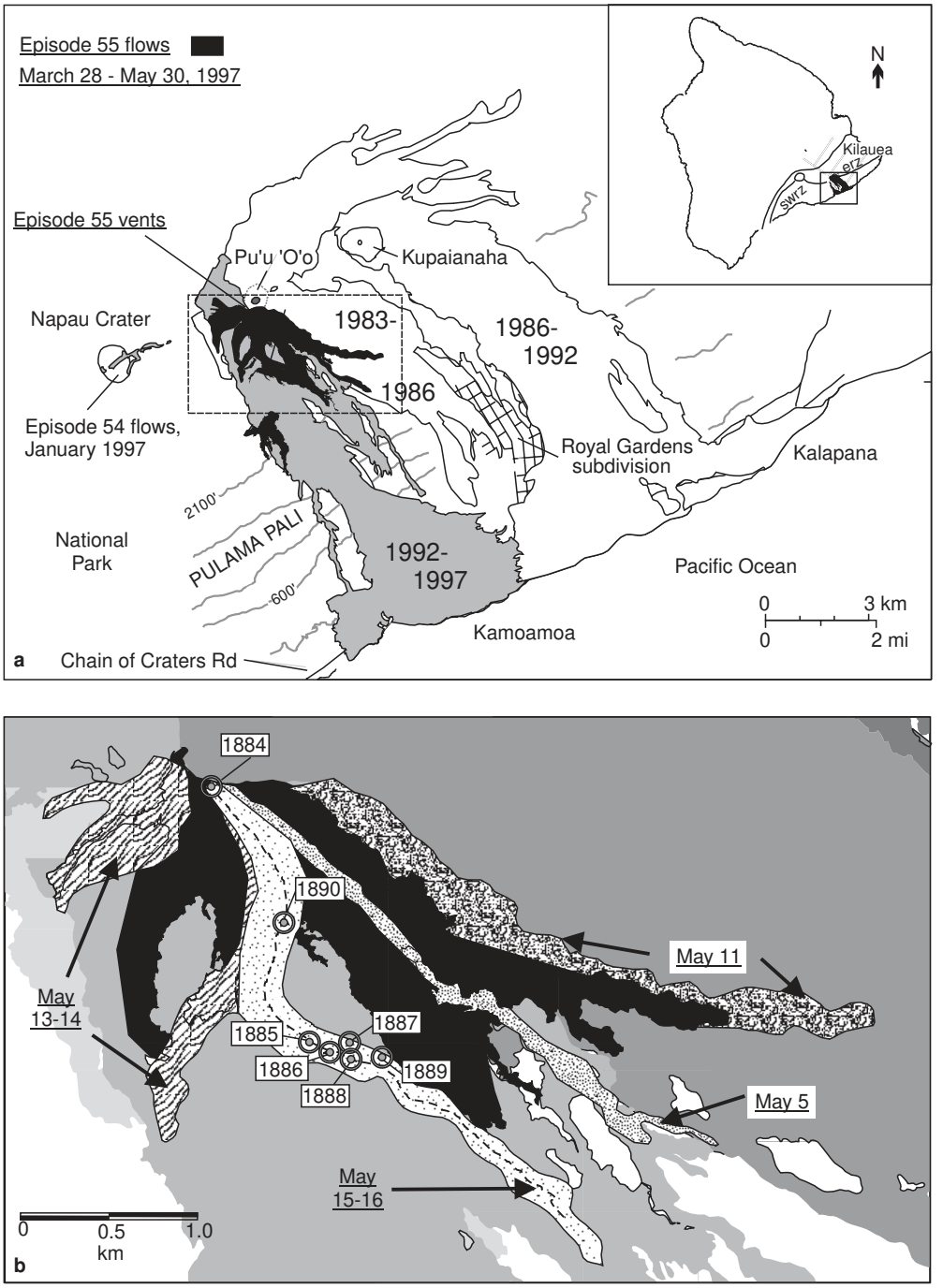

Fig. 2a Map of all flows emplaced during the 1983 to Present eruption of Kīlauea Volcano. Highlighted are the episode-55 vents and flows from which samples were collected. **b** Close-up of flow map showing individual flows emplaced from 5–6 May 1997. Included are sampling locations (*circles*) for the 15–16 May lava flow

outs from the main channel 0.9 km (KE55–1890), 1.85 km (KE55–1887) and 2.1 km (KE55–1889) from the vent. All secondary flows were sampled within 50–100 m of the active channel, and all samples (including those from the channel) were water quenched immediately after collection for optimal glass preservation. The secondary flow sample closest to the active vent was an overflow created by temporary blockage of the channel. It had a smooth silvery pāhoehoe surface, and its advancing flow lobes were thin (10–20 cm). The two samples collected farther down the flow were breakouts from the active channel, emerging from beneath the already present spinose ‘a‘ā surface crust. Both breakouts advanced slowly and were transitional in surface morphology. Flow fronts were thicker than those in the true pāhoehoe (20–30 cm high), and the flow surface was rough and typically broken into slabs during flow advance. Due to the inaccessibility of the vent itself on 16 May, we use a pāhoehoe cable-dip sample (KE55–1884) collected 2 days earlier from the base of the same vent as representative of lava erupted on 16 May.

Table 1 Glass analyses for all samples (all sample numbers have the prefix KE55-; last four numbers only are listed)

	1884 vent phh 0.05 km	1885 channel phh 1.7 km	1886 channel phh 1.8 km	1887 breakouttrans. phh 1.85 km	1888 channel ʻaʻā 1.9 km	1889 breakout trans.phh 2.1 km	1890 breakout phh 0.9 km
SiO_2	51.76 (0.26)	51.18 (0.27)	51.52 (0.17)	51.80 (0.35)	50.87 (0.38)	51.60 (0.31)	51.57 (0.15)
$A1_2O_3$	13.72 (0.11)	13.62 (0.08)	13.38 (0.09)	13.07 (0.16)	12.83 (0.56)	13.26 (0.14)	13.67 (0.07)
FeO	10.92 (0.15)	11.63 (0.29)	11.71 (0.15)	12.15 (0.54)	15.03 (0.57)	12.35 (0.27)	11.33(0.12)
MgO	6.76 (0.08)	6.40 (0.18)	6.27 (0.05)	6.06 (0.09)	4.25 (0.28)	6.18 (0.06)	6.66 (0.05)
CaO	10.69 (0.09)	10.95 (0.16)	10.35 (0.05)	10.35 (0.12)	9.11 (0.32)	10.49 (0.12)	10.34 (0.10)
Na_2O	2.31 (0.08)	2.30 (0.09)	2.42 (0.03)	2.37 (0.06)	2.37 (0.12)	2.38 (0.06)	2.48 (0.06)
TiO_2	2.44 (0.02)	2.60 (0.21)	2.70 (0.02)	2.86 (0.22)	3.49 (0.30)	2.80 (0.17)	2.57 (0.03)
MnO	0.16 (0.02)	0.16 (0.05)	0.17 (0.03)	0.18 (0.05)	0.22 (0.05)	0.19 (0.03)	0.18 (0.02)
K_2O	0.43 (0.01)	0.44 (0.03)	0.49 (0.01)	0.50 (0.03)	0.68 (0.06)	0.52 (0.03)	0.45 (0.01)
P_2O_5	0.24 (0.02)	NA	0.27 (0.02)	NA	NA	NA	0.26 (0.04)
Total	99.19	99.26	99.11	99.34	98.84	99.77	99.66
MgOT (°C)	1150	1142	1140	1136	1099	1138	1148
Glass	1.0	0.91	0.88	0.84	0.55	0.86	0.93
Pyroxene	tr	0.05	0.06	0.07	0.26	0.07	0.04
Plagioclase	tr	0.04	0.06	0.09	0.22	0.07	0.03
Olivine	<0.01	<0.01	<0.01	<0.01	<0.01	<0.01	<0.01

Standard deviation on ten spot analyses given in parentheses; USGS analyses include P_2O_5, University of Oregon analyses do not. Glass temperatures are calculated using MgO content (Helz and Thornber 1987) and phase proportions are calculated using phase compositions (from C.R. Thornber database) and mass balance

Analytical techniques

Electron probe microanalyzer (EPMA) glass compositions were analyzed at the University of Oregon on a Cameca SX-50 EPMA using 15 keV accelerating voltage, 10 nA beam current, and a ZAF data reduction routine. Glass and microlite compositions determined at the U.S. Geological Survey Denver Microbeam Facility were analyzed using a JEOL 8900 electron microprobe operating at 15 keV, 20 nA beam current, and a Phi-Rho-Zed data reduction routine. Alkali loss was minimized by use of a defocused (10–20 μm) beam. All reported glass compositions are averages of ten analyses, were collected from microlite-free regions, and were measured on the edge (best-quenched) portion of each sample. Analytical uncertainty in the MgO analyses used for glass geothermometry was 0.06–0.28 wt.%. These uncertainties led to uncertainties in calculated temperatures (using Helz and Thornber 1987) of 1.3–5.7 °C, respectively. Mass balance calculations used glass analyses from this study and microlite compositions from C.R. Thornber's database at HVO. Groundmass crystallinities for all samples were calculated using a weighted mass balance program (Table 1; M.B. Baker, pers. commun.), where the microlite-free vent glass was assumed to represent the initial melt composition for microlite crystallization of the channel samples.

Back-scattered electron imaging and textural analysis

Back-scattered electron (BSE) images were collected for all samples using a JEOL 6300V scanning electron microscope (SEM) at 10 keV, 5 nA beam current, and 15 mm working distance. Four to eight images were collected per sample from well-quenched areas of each thin section at magnifications of $\times 25$ (for examination of vesicles), $\times 200$, and $\times 500$ and analyzed using NIH Image 1.59. More images were used where crystal distribution was spatially heterogeneous (more common in poorly crystalline samples).

Plagioclase has a large atomic number contrast with the Fe-rich glass, allowing automated analysis of plagioclase area fraction and crystal number density (per area). Pyroxene number densities were analyzed by marking each crystal with a point followed by automated counting of those points. Total crystallinity (ϕ) was determined by point counting the BSE images, assuming that the measured area fraction of crystals is equivalent to the volume fraction. Direct comparison of plagioclase content determined by image analysis (area fraction) and mass balance (volume fraction) indicates that our method of imaging provides representative sample coverage (Fig. 3), despite obvious spatial heterogeneity in crystal distribution.

Measured areal number density (N_a) and ϕ values can be used to determine average crystal size ($d = k \cdot \sqrt{(\phi/N_a)}$, where k is a shape factor). Volumetric number density (N_v) can then be calculated as $N_v = N_a/d$ (Underwood 1970). We use this approximation rather than the more exact unfolding operations suggested by others (e.g., Higgins 1994; Pareschi et al. 1990; Peterson 1996; Sahagian and Proussevitch 1998), because other methods require full crystal size distribution measurements for all phases. We report both measured (two dimensional, N_a) and calculated (three dimensional, N_v) number density data for clarity and for ease of comparison with related studies (Table 2).

Table 2 Textural data for samples listed in Table 1

	pl N (mm^{-3})	d (mm)	pl $N_v \times 10^{-8}$ (cm^{-3})	px N_a(mm^{-3})	d (mm)	px $N_v \times 10^{-8}$ (cm^{-3})	$J_{pl} \times 10^{-5}$ (cm^3s)	$J_{px} \times 10^{-5}$ (cm^3s)
1885	478 (74)	0.009	0.53	2259 (572)	0.005	4.52	0.31	2.66
1886	1660 (80)	0.006	2.77	2729 (357)	0.005	5.46	1.54	3.03
1887	1560 (72)	0.007	2.20	2881 (264)	0.005	5.76	1.19	3.11
1888	4003 (621)	0.007	5.70	5515 (426)	0.006	9.19		
1889	1572 (60)	0.007	2.20	3252 (300)	0.005	6.51	1.05	3.10
1890	621 (98)	0.007	8.70	1561 (337)	0.005	3.12	0.97	3.47

Data given are measured plagioclase (pl) and pyroxene (px) areal number density (N_a), average linear size ($d = (\phi/N_a)^{2/1/2}$), where ϕ for each phase is that calculated by mass balance and listed in Table 1; volumetric number density (N_v), calculated as N_a/d and converted to no./cm^3, and nucleation rate (J), calculated assuming an average flow velocity of 1 m/s

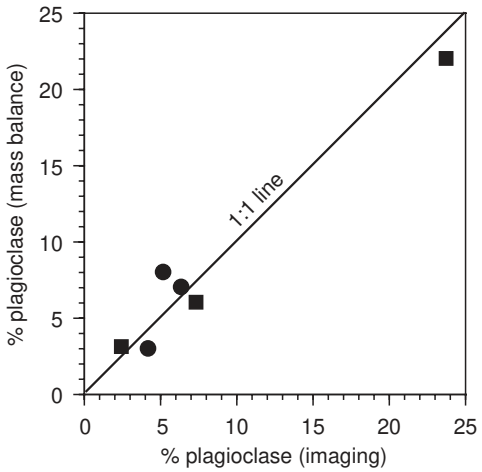

Fig. 3 Comparison of plagioclase abundance measured by imaging (area %) and by mass balance (volume %). *Squares* represent the channel sequence, *circles* the breakout sequence. Measurements were used to insure that images collected were representative of the sample as a whole

Observations of cooling and crystallization during flow through open channels

Qualitative description of sample textures

Vent samples are highly vesicular and nearly aphyric, characterized by minor (<1%) olivine phenocrysts in a clear brown glass. Vent samples also have rare (≪1%) small (<10 μm) plagioclase and clinopyroxene microlites (Fig. 4a), indicating that the lava temperature and composition were located near the plagioclase–pyroxene cotectic at the time of eruption. Cooling and crystallization during flow generate abundant microlites of plagioclase and clinopyroxene in all flow samples (Fig. 4b). Plagioclase microlites are typically acicular in two-dimensional cross section, indicating their true form to be thin tablets (Higgins 1994). Pyroxene microlites are smaller, more numerous, and more equant (in two dimensions) than plagioclase microlites, reflecting prismatic shapes in three dimensions. Pyroxene crystals commonly nucleate on plagioclase microlites and on vesicle walls (Fig. 4c). In less crystalline samples, the spatial distribution of crystals is heterogeneous, with microphyric aggregates of intergrown plagioclase and pyroxene separated by larger pockets of glass. Also common are intricate intergrowths of plagioclase and pyroxene (Fig. 4d) that resemble crystal habits typical of high cooling rates (Lofgren 1980; Lesher et al., in press).

All samples show an increase in crystallinity with increasing distance from the vent (Fig. 5). Channel sample KE55–1885, collected 1.7 km from the vent, is poorly crystalline (9%; Table 1), and microlites are spatially heterogeneous, with plagioclase and pyroxene microlite aggregates in otherwise crystal-free glass (Fig. 5a). Sample KE55–1886, collected 100 m down channel from KE55–1885 and directly below a small lava falls, has a somewhat higher crystallinity (12%; Fig. 5b), with both plagioclase and pyroxene microlites more abundant. The ‘a‘ā channel sample is highly crystalline (45–50%), with intergrown laths of plagioclase and pyroxene forming a spatially homogeneous crystalline texture (Fig. 5c). Samples collected from channel overflows and breakouts also increase in crystallinity with distance from the vent (Fig. 5d–f). The most proximal sample in the suite (Fig. 5d), collected ~1 km from the vent, is highly vesicular and sparsely crystalline (~7%). Samples collected from channel breakouts immediately above (Fig. 5e) and 200 m below (Fig. 5f) the pāhoehoe-‘a‘ā transition are similar in texture to each other and to the channel sample collected 1.8 km from the vent (Fig. 5b), with crystallinities of ~15%. Thus, the channel breakout 2.1 km from the vent (Fig. 5f) is substantially less crystalline than the surface ‘a‘ā sample collected at 1.9 km (Fig. 5c). The breakout provides a sample of the flow interior, so its low crystallinity relative to that of the flow surface indicates a change in thermal structure from homogeneous (well stirred) in the proximal channel to thermally stratified in medial to distal areas (e.g., Crisp and Baloga 1990; Kilburn 1996).

All channel and breakout samples are highly vesicular. Vesicles in pāhoehoe are distinct from those in ‘a‘ā, however, in both shape and interior roughness. Pāhoehoe vesicles are spherical to ellipsoidal (Fig. 6a) and show little interconnection. ‘a‘ā vesicles are highly irregular in shape, extensively interconnected, and have

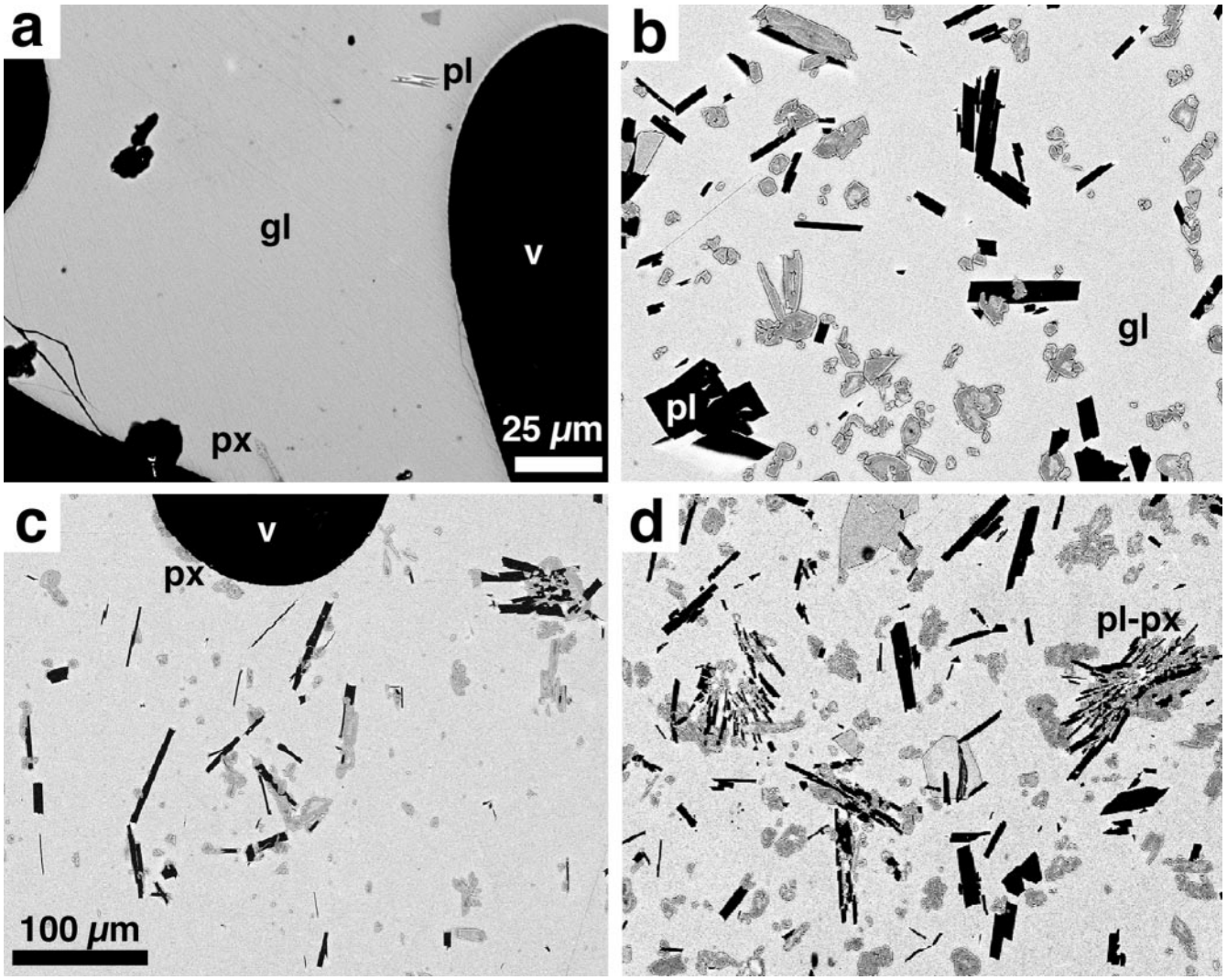

Fig. 4a Back-scattered electron (BSE) image of vent sample KE55–1884. Labeled are vesicles (*v, black*), plagioclase (*pl* or *plag, dark gray*), pyroxene (*px, medium gray*), and glass (*gl, light gray*). **b** Typical texture of downflow samples as illustrated by KE55–1889. Scale is same as in **a**. **c** Illustration of nucleation of pyroxene on vesicle walls, as seen in KE55–1890. **d** Plagioclase–pyroxene aggregates (*pl-px*) in KE55–1889. Scale is same as in **c**

rough interfaces as a consequence of abundant microlites (Fig. 6b). These vesicle characteristics are consistent with other descriptions of pāhoehoe and ‘a‘ā flow textures (Macdonald 1953; Walker 1989; Crisp et al. 1994; Cashman et al. 1994; Polacci and Papale 1997), and reflect the high viscosity (long bubble relaxation times) of ‘a‘ā lavas (Polacci et al. 1999).

Analysis of sample textures and phase compositions

Glass geothermometry and sample crystallinity The composition of glass quenched during lava sampling provides a direct measure of sample temperature and, when referenced to an initial bulk composition, sample crystallinity. In particular, the MgO content of basaltic melt decreases linearly with temperature throughout much of the crystallization interval as a consequence of preferential incorporation of MgO into growing olivine or pyroxene. MgO thus provides an effective measure of the temperature to which a lava is equilibrated by crystallization prior to quenching (Helz and Thornber 1987; Montierth et al. 1995). These experimental calibrations have been tested using samples from active flows of known temperatures (Helz et al. 1995; Montierth et al. 1995). Calculated temperatures are within 10 °C of temperatures determined in the field, except where the erupted magma is volatile rich and effectively undercooled relative to atmospheric conditions (e.g., Lipman and Banks 1987; Montierth et al. 1995). There may be a small kinetic lag time between cooling and crystallization in response to that cooling, so that glass geothermometry temperatures are considered to yield *maximum* temperatures (and thus minimum cooling rates) for lava samples.

All 16 May samples have bulk compositions similar to those of samples collected during intervals of steady

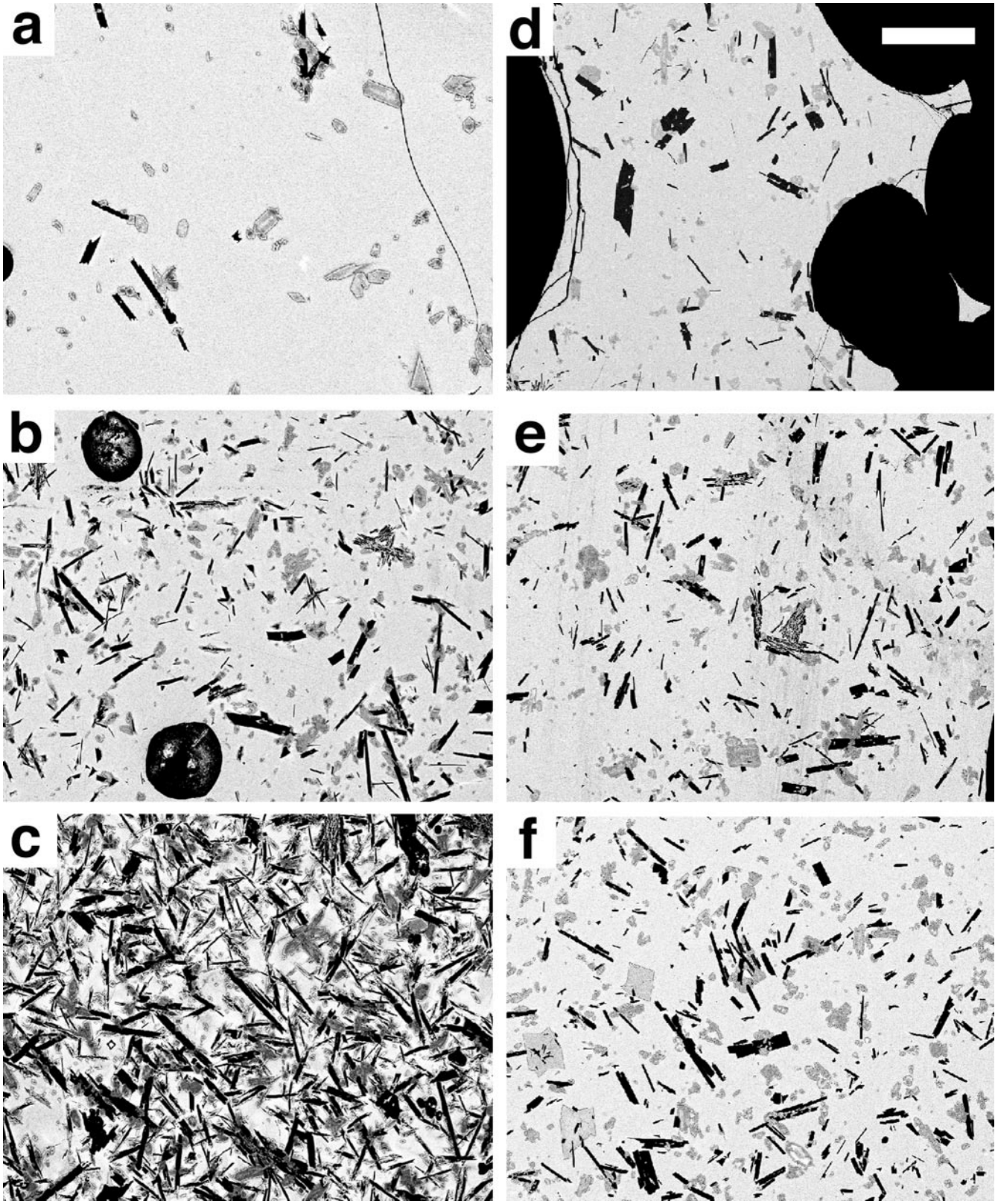

Fig. 5 Typical BSE images illustrating **a–c** textural changes in channel and **d–f** breakout sample sequences. *Scale bar* shown in **d** is 100 μm and is the same for all images. **a** KE55–1885; **b** KE55–1886; **c** KE55–1888; **d** KE55–1890; **e** KE55–1887; **f** KE55–1889

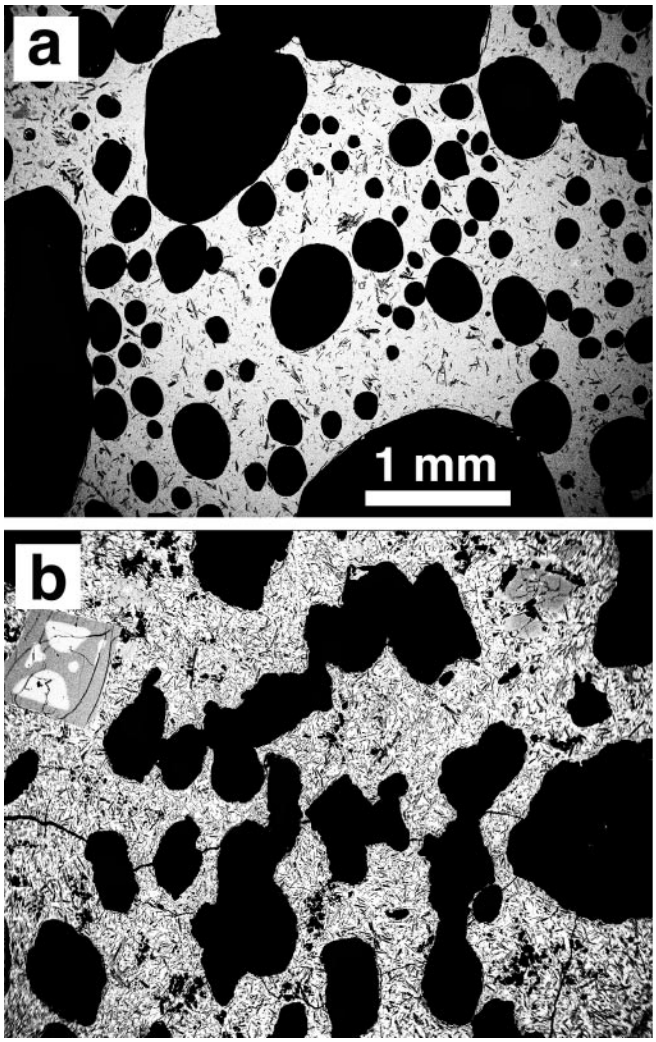

Fig. 6 Typical vesicle textures for **a** pāhoehoe (KE55–1890) and **b** ‘a‘ā (KE55–1888) samples. *Scale bar* is the same for both images. Note both the irregularity and the connectivity of the vesicles in the ‘a‘ā sample

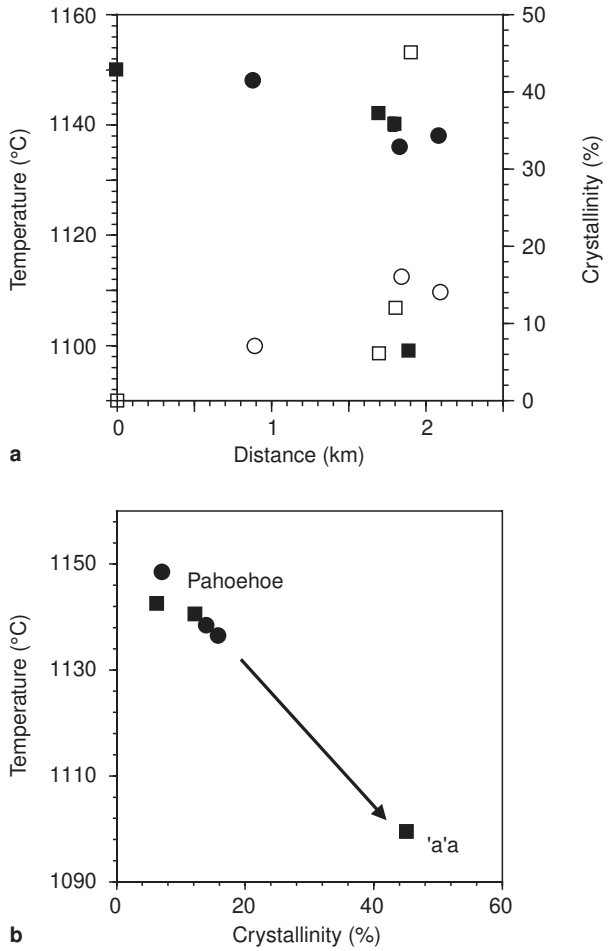

Fig. 7a Changes in sample crystallinity (*open symbols*) and glass temperature (*filled symbols*) with increasing distance from the vent. **b** Change in glass temperature (calculated using wt.% MgO) with sample crystallinity (calculated using mass balance of all major elements). In both **a** and **b**, *squares* represent the channel sequence, *circles* the breakout sequence

activity in episodes 48 through 53 (e.g., Helz et al. 1991; Mangan et al. 1995; Thornber et al. 1996; Heliker et al. 1998). The glass composition of the vent sample indicates that the eruption temperature was also similar to those of previous episodes. Vent glass from May 1997 has an average MgO content of 6.75 wt.% (equivalent to an eruption temperature of 1149 °C using the calibration of Helz and Thornber 1987). This MgO-based temperature is comparable to average values for episode 53 (6.9 wt.% MgO; 1153 °C), episodes 50–52 (6.94 wt.% MgO; 1153.5 °C), and episode 49 (6.82 wt % MgO; 1151 °C).

With flow, sample crystallinities increase and glass temperatures decrease (Fig. 7a). Channel pāhoehoe samples 1.7 and 1.8 km from the vent have average temperatures of 1142 and 1140 °C. These temperatures are identical within analytical error (±1.30 °C), but the clear difference in crystallinity between these samples (volume fraction $\phi = 0.09$ and 0.12, respectively; Fig. 5a,b) demonstrates that the glass geothermometer provides a reasonable estimate of relative quench temperatures among samples. Consistent with its high crystallinity ($\phi = 0.45$), the ‘a‘ā sample has a much lower glass-based temperature of 1099 °C. Overflow and breakout samples have glass temperatures of 1148 °C at a distance of 0.9 km from the vent, and 1136–1138 °C at distances of 1.85–2.1 km from the vent, and corresponding crystallinities of 0.07, 0.16, and 0.14, respectively. These are minimum temperatures (maximum crystallinities), because we cannot discount the possibility that some cooling and crystallization occurred during flow from the channel to the sampling location. However, the close correlation between channel and breakout samples indicates that extensive crystallization did not occur over the short (< 100 m) distances of surface flow.

MgO-based temperatures and sample crystallinities are compared in Fig. 7b. The approximately linear relationship between lava temperature and crystallinity is

consistent with that suggested by Shaw (1969) based on his experiments and with cotectic precipitation of plagioclase and pyroxene. This linear relationship breaks down at higher crystallinities (lower temperatures), as ilmenite and magnetite join the crystallizing assemblage (Wright and Okamura 1977).

Rates of cooling and crystallization

Rates of flow cooling and crystallization can be estimated by combining measured down-channel changes in flow temperature and crystallinity with observed flow velocities. For these estimates, breakout samples are assumed to represent channel lava at an equivalent distance from the vent. Cooling rates of 4.4–6.8 °C/km characterize flow through the proximal portion of the channel. These rates translate to 0.004–0.014 °C/s (Table 2), assuming an average flow velocity of 1–2 m/s. Rates of bulk crystallinity increase are 0.05–0.08 volume fraction per kilometer ($0.5–0.8 \times 10^{-4}$ ϕ/s for an average channel velocity of 1 m/s). The ‘a‘ā sample was omitted from these calculations, because we did not measure channel-margin velocities; however, we can estimate margin velocities using the rates determined above. To achieve the observed ‘a‘ā temperature of 1099 °C and crystallinity of 0.45 (Table 1), the average flow velocity along the channel margins must have been ~0.34–0.5 m/s, less than half the centerline channel velocity.

Our estimates can be compared with rates of cooling and crystallization measured in the much larger ‘a‘ā flows produced during the 1984 eruption of Mauna Loa (Lipman and Banks 1987; Crisp et al. 1994). Here transport of lava through stable channels (calculated for two separate days, 31 March and 6 April 1984) led to a 5–7 °C drop in temperature over 10–11 km of transport. This yields a cooling rate of 0.004 °C/s, assuming average flow rates of 5 m/s (records from stations along the channel show velocities to drop from 15 m/s at the vent to 2 m/s at a distance of 10 km). Crystallization rates for the same samples were 0.01–0.04 volume fraction ϕ/km, or $0.4–1.0 \times 10^{-4}$ ϕ/s, also comparable to rates determined for the Kīlauea channel. Thus, rates (per time) of cooling and crystallization are similar in the small Kīlauea 1997 flow (effusion rates ~3–4 m^3/s) and the large Mauna Loa 1984 flow (effusion rates ~100 m^3/s) despite different channel velocities. This similarity suggests that observed cooling rates of ~0.005 °C/s and crystallization rates $\sim 0.5 \times 10^{-4}$ ϕ/s may be typical of most proximal to medial open-channel Hawaiian flows (particularly those erupted at near-cotectic temperatures). In contrast, cooling rates of ~1 °C/km typify flow through lava tubes (Peterson and Swanson 1974; Cashman et al. 1994). These rates translate to cooling rates of 0.001–0.002 °C/s for assumed average flow velocities of 1–2 m/s (e.g., Kauahikaua et al. 1998), two to four times lower than cooling rates of open-channel flows.

Modes of crystallization

Crystallization can occur through nucleation of new crystals, by growth on existing nuclei, or through a combination of the two processes. In general, nucleation is assumed to dominate when supersaturations are high, whereas crystal growth is considered more important in systems experiencing only small deviations from equilibrium. However, measurement of supersaturation is difficult in multi-component systems. Thus textural data (crystal size, number density, and abundance) provide unique information on conditions of crystallization.

The number of both plagioclase and pyroxene microlites increases steadily down channel (Fig. 8a). This steady increase implies a constant rate of both plagioclase and pyroxene nucleation through time, if flow velocities were constant. Nucleation rates estimated from Fig. 8a are $\sim 1.5–3 \times 10^5$/cm^3s for pyroxene and $0.3–1.5 \times 10^5$/cm^3 s for plagioclase, when calculated assuming an average channel velocity of 1–2 m/s (Table 2). For comparison, crystal nucleation rates estimated from textural measurements on samples from the Mauna Loa 1984 flow (Crisp et al. 1994) are $0.84–3.4 \times 10^5$/cm^3s for pyroxene and $0.1–0.5 \times 10^5$/cm^3s for plagioclase.

Neither the 1984 Mauna Loa nor the 1997 Kīlauea sample suite show evidence for the $\sim 10^4$ s crystallization delay commonly assumed for plagioclase crystallization in basaltic melts at moderate cooling rates (Uhlmann et al. 1979). However, the plagioclase data suggest a small delay in plagioclase nucleation relative to that of pyroxene. A linear fit to the data in Fig. 8a shows that plagioclase number densities intersect the x-axis at ~0.4 km, implying a delay in plagioclase nucleation of < 400 s, despite the rare plagioclase microlites in the vent sample (Fig. 4a). This delay is comparable to nucleation delays achieved under very high rates of cooling in experiments on comparable compositions (~1000 °C/h; Lesher et al., in press). The apparent decrease in plagioclase incubation time relative to static experiments confirms the importance of dynamical effects (stirring) on crystal nucleation (e.g., Kouchi et al. 1986).

On a plot of N_a vs ϕ (Fig. 8b), straight lines through the origin connect samples with a constant average crystal size (area) and indicate that crystal nucleation is largely responsible for the overall increase in sample crystallinity. Nucleation-dominated crystallization typifies both plagioclase and pyroxene formation in all pāhoehoe samples (Fig. 8b), although average plagioclase crystal areas of 48 μm^2 are twice those of pyroxene (~23 μm^2) in the same samples. High plagioclase and pyroxene number densities in the ‘a‘ā sample demonstrate the continued importance of nucleation in the crystallization of both phases, although the observed doubling of the average pyroxene size (to 47 μm^2) reflects the increasing importance of crystal growth.

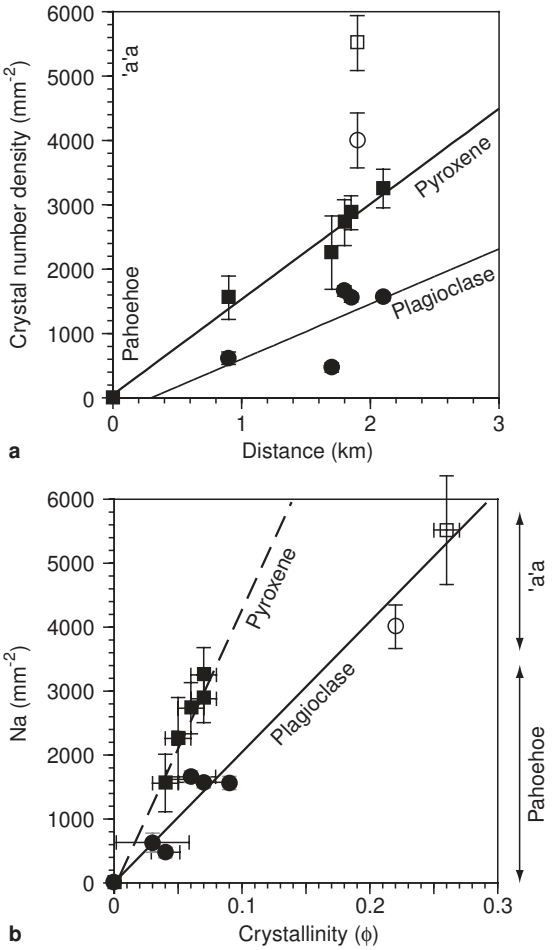

Fig. 8a Changes in plagioclase (*circles*) and pyroxene (*squares*) crystal number density (N_a) with increasing distance from the vent. *Filled symbols* are pāhoehoe samples, *open symbols* 'a'ā. **b** Number density (N_a) vs phase crystallinity (ϕ) for both plagioclase and pyroxene. *Solid line* shows best fit to pāhoehoe plagioclase data and represents an average crystal area of 40 μm^2. *Dashed line* shows best fit to pāhoehoe pyroxene data and represents an average crystal area of 28 μm^2

Plagioclase number densities $>1000\,mm^{-3}$ have been reported for other 'a'ā surface and flow interior samples (e.g., Crisp et al. 1994; Polacci et al. 1999). In fact, high crystal number densities appear characteristic of 'a'ā emplacement styles and contrast with the consistently low number densities that typify fully crystallized pāhoehoe flows ($\leq 10^2/mm^2$; Sato 1995; Katz 1997). Based on the data reported above, we suggest that high crystal number densities are the direct result of high rates of cooling (and crystal nucleation) in proximal 'a'ā channels.

Discussion

Data presented herein can be used to constrain parameters used in models of lava flow cooling during transport through open channels and to extend existing models for the pāhoehoe-'a'ā transition.

Rates of cooling and crystallization

Cooling rates

Measured rates of cooling during flow through the 16 May channel can be compared with model predictions. We use the heat balance proposed by Crisp and Baloga (1994) to calculate cooling rates of the flow interior. The flow was well stirred, and entrained crust was of negligible thickness in proximal regions of the channel; thus, we simplify that heat balance as

$$dT/dt = (L/C_p)(d\phi/dt) - (\varepsilon\sigma f T^4)/\rho C_p h \quad (1)$$

by assuming perfect mixing and neglecting the effects of entrainment and assimilation, where L is the latent heat of crystallization (350,000 J kg^{-1}), Cp is the heat capacity (1200 $Jkg^{-1}K^{-1}$), $d\phi/dt$ is the crystallization rate ($0.5–0.9\times10^{-4}$/s for a channel velocity of 1 m/s, as shown above), ε is emissivity (0.9), σ is the Stefan-Boltzmann constant ($5.67\times10^{-8}\,Jm^{-2}s^{-1}K^{-4}$), f is the fraction of core exposed, T is the lava temperature in degrees Kelvin (K), ρ is lava density (2000 kg m^{-3} assumed based on observed sample vesicularity), and h is flow thickness. Equation (1) can be integrated to solve for time (in seconds) to reach a given T (in K) as

$$t = [k/2a]\cdot\{(0.5)\ln[(T+k)/(T-k)] + \tan^{-1}(T/k)\} + A, \quad (2)$$

where $a = (L/C_p)(d\phi/dt)$, $k = (-a/b)^{1/4}$, with $b = -\varepsilon\sigma f/C_p h$, and A is a constant of integration calculated for the initial condition t = 0, T = 1422 K.

Rates of cooling with distance traveled may be calculated if time (calculated from Eq. 2) is converted to distance by assuming a flow velocity (here chosen as 1 m/s). The results of such calculations are shown in Fig. 9 for reasonable parameter values for the variables *f, h,* and $d\phi/dt$. Observed cooling rates can be matched for a flow depth h of 3 m (the maximum allowed by field observations) for the conditions $d\phi/dt = 0.5\times10^{-4}$/s and $f = 0.7$, or $d\phi/dt = 0.7\times10^{-4}$/s and $f = 0.9$ (curve C; Fig. 9). For a shallower flow depth (2 m), bracketing crystallization rates of 0.5×10^{-4}/s and 0.9×10^{-4}/s require, respectively, crustal coverage f of 0.5 and 0.7 (curves D and B). High crystallization rates and small fractions of exposed core generate too much heat for adequate flow cooling (e.g., curve A), whereas lower crystallization rates, smaller flow depths, or high values of f predict too much cooling (e.g., curve E).

These calculations are only approximate but provide an adequate match to high rates of cooling (0.004–0.007 °C/s, or 14–25 °C/h, for an assumed velocity of 1 m/s) measured during flow through the proximal channel. Thus, we suggest that, for early stages of flow through an open channel, cooling rates of flow interiors approach those of purely radiative heat loss from perfectly mixed flows. That all of our measured tempera-

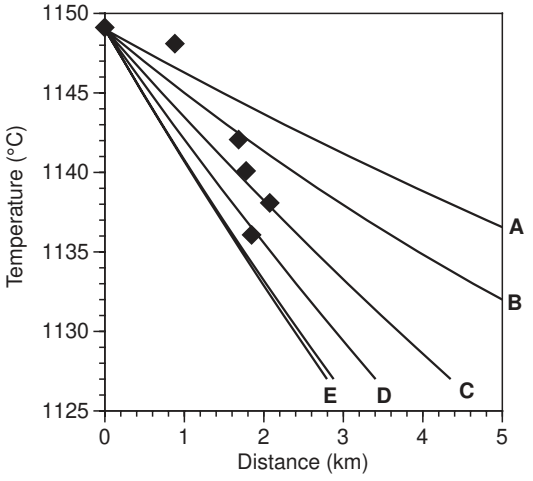

Fig. 9 Cooling times calculated using Eq. (2) and converted to distance traveled assuming an average flow velocity of 1 m/s (data from Fig. 7a shown for comparison) Curves calculated under the following conditions: *A* h = 3 and either $d\phi/dt = 0.5 \times 10^{-4}$, f = 0.6 or $d\phi/dt = 0.7 \times 10^{-4}$, f = 0.8; *B* h = 2, $d\phi/dt = 0.9 \times 10^{-4}$, f = 0.7; *C* h = 3 and either $d\phi/dt = 0.5 \times 10^{-4}$, f = 0.7 or $d\phi/dt = 0.7 \times 10^{-4}$, f = 0.9; *D* h = 2, $d\phi/dt = 0.5 \times 10^{-4}$, f = 0.5; *E* h = 3 and either $d\phi/dt = 0.5 \times 10^{-4}$, f = 0.8 or $d\phi/dt = 0.7 \times 10^{-4}$, f = 1

tures do not follow a single curve in Fig. 9 probably reflects both decreasing flow velocities and increasing crustal coverage down channel.

Crystallization rates

Cooling leads to crystallization. Thus, the 16 May sample suite allows us to determine the effects of high cooling rates on the kinetics of crystallization. In general, rapid cooling is expected to result in high rates of crystal nucleation (e.g., Cashman 1993), consistent with the high observed crystal number densities in all samples. Are nucleation rates greater than anticipated from rapid cooling alone, as suggested by experimental results of Emerson (1926), Kouchi et al. (1986), and Sato (1995)? Plagioclase number density (N_v) and cooling rate (CR) can be related empirically as

$$\log N_v(\mathrm{cm}^{-3}) = 0.94 \log \mathrm{CR}(^\circ\mathrm{C/hr}) + 6.7 \quad (3)$$

using textural data from small basaltic dikes (e.g., Cashman 1993). This calibration (Eq. 3) works well for relating measured plagioclase number densities (N_v) to cooling rates in pāhoehoe flows, where cooling of the flow interior is dominated by conduction (Montierth and Cashman 1996). However, based on this calibration, plagioclase number densities (N_a) in ‘a‘ā of $\sim 4000\ \mathrm{mm}^{-2}$ ($N_v \sim 6.3 \times 10^8\ \mathrm{cm}^{-3}$) imply average cooling rates of $\sim 170\,^\circ$C/h, 3.5 times the maximum cooling rate measured for the 16 May flow (and nearly eight times the average). This discrepancy supports experimental evidence that physical aspects of flow stirring act to enhance rates of crystal nucleation. In industrial crystallization, this phenomenon is referred to as “secondary nucleation” and may be a consequence of either mechanical or physico-chemical processes (e.g., Mullin 1976).

Thermal structure of ‘a‘ā flow interiors

High rates of cooling and crystallization should lead to rapid solidification (in $\sim 10^4$ s). That ‘a‘ā flows persist over times greatly in excess of a few hours and generate flow lengths of tens of kilometers shows that these very high rates of cooling are not maintained. In fact, ‘a‘ā flow models commonly assume a thermal structure that involves two components: a crust that cools by radiation and thickens with time, and an isothermal core (e.g., Crisp and Baloga 1990). This thermal structure leads to a flow with two mechanically distinct components (Kilburn 1996).

In the 1997 Kīlauea flow, the pāhoehoe-‘a‘ā transition marked the location where the thermal structure of the flow changed from well mixed to thermally stratified. Above the transition, stirring of lava in the channel became less vigorous below a lava falls ~ 1.75 km from the vent, allowing a thin crust to form over the central part of the channel. Below 1.9 km, the location of the pāhoehoe-‘a‘ā transition, most of the flow surface was covered by a spinose ‘a‘ā crust. Thermal stratification is illustrated by the similarity in both temperature and crystallinity between breakouts from the flow interior sampled above and below the transition, and by the disparity between these samples and the overlying ‘a‘ā crust. Thus, a critical component of any lava flow model must be the parameterization of changes in the thermal structure of the flow from well mixed to thermally stratified.

Once thermally stratified, ‘a‘ā flow interiors cool slowly. As a consequence, breakouts from flow interiors commonly have transitional pāhoehoe surface morphologies (Wolfe et al. 1988; Kilburn 1990; Jurado-Chichay and Rowland 1995) and nearly constant temperatures (e.g., Neal et al. 1988; Calvari et al. 1994; Calvari and Pinkerton 1998). Sampling such breakouts may be the best way to track core temperatures with distance, thus providing a means of obtaining flow temperature–distance relations necessary for the application of flow cooling models and for predicting lengths of active flows (e.g., Pinkerton and Wilson 1994).

Transitions in flow surface morphology

The surface morphology of ‘a‘ā flows changes with increasing distance traveled (e.g., Macdonald 1953). Our data suggest that these changes (from smooth pāhoehoe to transitional pāhoehoe to ‘a‘ā) are correlated with increases in lava crystallinity, as the addition of crystals to a melt will change the lava rheology and may ultimately inhibit viscous flow. Examination of this cor-

relation requires a brief review of the effect of particles on the rheology of fluids.

Suspension rheology

The particle volume fraction at which maximum packing (ϕ_m) is achieved controls the change from fluid to solid behavior. At $\phi < \phi_m$ a particle-melt suspension has a viscosity that increases with increasing ϕ. The increase in suspension viscosity (h_s) relative to the liquid viscosity (h) with increasing particle volume fraction (ϕ) is scaled to ϕ_m as

$$\eta_s/\eta = (1-(\phi/\phi_m))^{-[\eta]\phi m}, \quad (4)$$

where $[\eta]$ is the intrinsic viscosity and $[\eta]\phi_m$ reflects the extent to which particles interact (Krieger and Dougherty 1959). In geologic applications, $[\eta]\phi_m$ is commonly assumed to be 2.5 (the Roscoe-Einstein equation) and ϕ_m is considered to be a geometric constant of 0.6 (e.g., Marsh 1981; Pinkerton and Stevenson 1992). However, experimental studies show that both $[\eta]$ and ϕ_m may vary with crystal shape, resulting in variations in the exponent $[\eta]\phi_m$ from, e.g., 1.31 for glass fibers to 3.77 for glass plates (Barnes et al. 1989). Exact values of ϕ_m will also vary with changes in particle size distribution, as a range of particle sizes often permits more efficient packing (higher ϕ_m) than possible for uniform particle populations (e.g., Barnes et al. 1989; Probstein et al. 1994). Finally, ϕ_m may vary with increases in applied stress, which will affect the orientation and packing of non-equant crystals (Fig. 10a; Wildemuth and Williams 1984, 1985).

The addition of particles to a suspension will also lead to non-Newtonian behavior, particularly Bingham flow. A fluid shows Bingham behavior when a minimum stress (the yield strength, τ_y) must be exceeded for viscous flow to occur. A yield strength develops when particles in a suspension form a "touching framework" (Kerr and Lister 1991), and the yield strength is measured by the stress required to disrupt that framework. In suspensions, two particle volume fractions ($\phi_{m,0}$ and $\phi_{m,\infty}$) bracket conditions for Bingham flow. At $\phi_{m,0}$, the minimum ϕ at which a suspension first exhibits yield strength behavior, very small applied stresses are sufficient to disrupt the incipient particle network and permit viscous flow (i.e., τ_y approaches 0; Fig. 10b). In contrast, $\phi_{m,\infty}$ designates the maximum packing possible for a specific collection of particle sizes and shapes under any applied stress and represents the ϕ above which the suspension will not flow under any external force (Fig. 10b; Zhou et al. 1995). A suspension will exhibit Bingham behavior for the condition $\phi_{m,0} < \phi_m < \phi_{m,\infty}$. Both $\phi_{m,0}$ and $\phi_{m,\infty}$ will be determined by the viscosity of the suspending medium, the specific particle size and shape distribution, and the form of applied stress (compression vs shear).

Yield strength and the transition to 'a'ā

There is general agreement in the geological literature that basaltic crystal-melt suspensions start to exhibit non-Newtonian (Bingham) behavior at minimum crystallinities ($\phi_{m,0}$) of 0.25–0.30, that most possess a yield strength when crystallinities exceed ~0.4, and that viscous flow is impossible for $\phi(=\phi_{m,\infty}) > 0.6$ (Shaw et al. 1968; Shaw 1969; Pinkerton and Stevenson 1992; Lejeune and Richet 1995; Pinkerton and Norton 1995;

Fig. 10a,b Illustration of rheological changes occurring with increasing crystallinity, based on Eq. (4). **a** Changes in relative viscosity (η_s/η) with increasing crystallinity (ϕ). Curves 1 and 2 are from data in Zhou et al. (1995) for a suspension of silica powder in aqueous glycerine and are presented as an example of the effect of applied stress (τ) on the packing limits of a suspension. *Curve 1:* $\tau = 3.3$ Pa; $\phi_m = 0.383$; $[h]\phi_m = 0.92$. *Curve 2:* $\tau = 700$ Pa; $\phi_m = 0.529$; $[\eta]\phi_m = 2.10$. *Curve 3* shows the commonly used Roscoe-Einstein formulation for viscosity, with $\phi_m = 0.6$ and $[h]\phi_m = 2.5$. **b** Illustration of the relation between crystallinity (ϕ) and shear stress (τ) in determining the onset of Bingham flow behavior (after Zhou et al. 1995). $\phi_{m,0}$ is the lowest crystallinity for a given particle population at which the suspension exhibits a yield strength (low stress limit); $\phi_{m,\infty}$ is the maximum packing at which viscous flow is possible under any applied stress. The suspension exhibits Bingham behavior over crystallinities of $\phi_{m,0} > \phi_m > \phi_{m,\infty}$

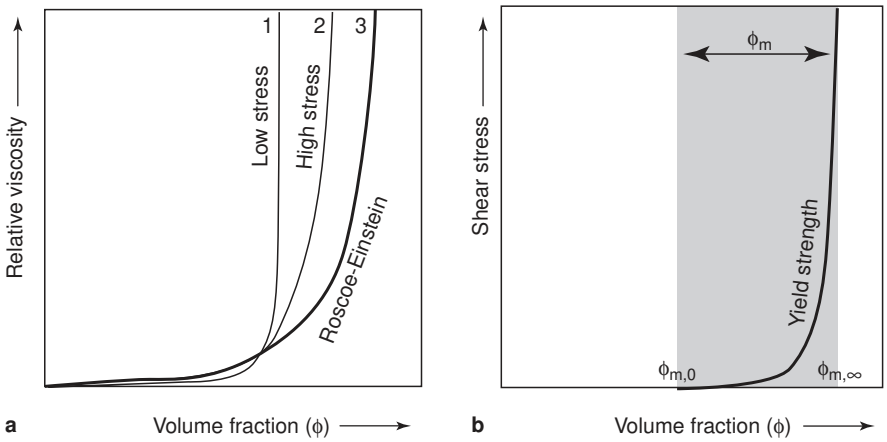

Hallot et al. 1996; Smith 1997; Philpotts et al. 1998). To what extent do these rheological thresholds control the pāhoehoe-'a'ā transition?

Maximum groundmass crystallinities measured in 'a'ā range from ~0.45 (our data) to 0.53–0.59 (Crisp et al. 1994). The common description of 'a'ā formation by "tearing" of the flow surface implies a response to deformation that does not involve viscous flow. On the basis of these data and the shear stress (τ)-crystallinity (ϕ) relations illustrated in Fig. 10b, we suggest that 'a'ā forms as the crystallinity of the flow surface approaches ϕ_m for the local conditions of applied stress. Here the initial tearing of the flow surface results when microlite crystallinity is sufficient to inhibit continuous flow in response to shear. For the moderate to high shear stresses expected in open channel flows, this condition can occur only for moderately high crystallinities (e.g., above the bend in the τ_y–ϕ curve of Fig. 10b).

The association of 'a'ā flow behavior with that of a fluid possessing a yield strength is not new. Robson (1967) and Walker (1967) first made this observation by noting that Etnean flows thickened with increasing distance from eruptive vents. Since this time, measurements of flow rheologies (e.g., Pinkerton and Sparks 1978; Fink and Zimbelman 1986, 1990; Moore 1987; Pinkerton and Norton 1995) have confirmed non-Newtonian behavior of some basaltic lava flows, and flow models assuming Bingham behavior have been developed (e.g., Hulme 1974; Dragoni 1989; Dragoni and Tallarico 1994). Additionally, both Peterson and Tilling (1980) and Kilburn (1990) allow for Bingham behavior in basing their strain rate–viscosity models (Fig. 1) on observed increases in the *apparent* viscosity of the lava, a statement that encompasses a wide range of true fluid rheologies. Defining the pāhoehoe-'a'ā transition in the context of ϕ_m, the yield strength dictating limits to viscous flow, is thus a logical extension of previous models (Fig. 1; e.g., Peterson and Tilling 1980; Kilburn 1981, 1990, 1993, 1996). Such a definition also provides a physical explanation for the threshold nature of the transition.

Toward a general model for transitions in flow morphology

Transformation of the 16 May flow surface to 'a'ā apparently required both flow stirring that was sufficiently vigorous to prevent extensive surface crust formation and crystal–crystal interactions that were sufficiently strong to prohibit viscous deformation of the flow surface under the applied shear stress. Are these necessary conditions for 'a'ā formation, are they sufficient to guarantee 'a'ā formation, and can they be generalized?

If the answers to the first two questions are affirmative, we can start to develop a general framework for predicting basaltic lava flow behavior. In laminar flow experiments, crustal stability may be represented by a single dimensionless parameter Ψ, a ratio of relative time scales of flow surface cooling (τ_s) and flow advection (τ_a; Fink and Griffiths 1990, 1992; Griffiths and Fink 1993). While not directly applicable to well-stirred open channel flows, a parameterization of this form (Ψ') could potentially define limiting conditions for stable crust formation. Rates of crustal recycling, in turn, control the rates at which flow interiors cool and crystallize. Flow crystallinity (ϕ) determines flow rheology, and is most usefully defined with reference to specific rheological transitions (e.g., $\phi/\phi_{m,\infty}$).

Figure 11 presents a schematic illustration of conditions leading to pāhoehoe and 'a'ā flow surface formation using the dimensionless parameters suggested previously. Smooth pāhoehoe forms when fluid yield strengths are negligible and rates of crustal recycling are low, so that crust formation dominates emplacement (low Ψ'). The pāhoehoe has a rough, transitional surface when crystallinities are moderate and yield strengths are sufficiently large to prevent relaxation of small-scale surface roughness over short chilling times (~10^2 s). 'A'ā surface formation requires that Ψ' is sufficiently high to prevent continuous crust formation and that yield strength is sufficiently high to prevent viscous flow. Thus, 'a'ā will probably be restricted to a relatively small crystallinity range ($\phi > \sim 0.7\phi_{m,\infty}$?). Morphologic transitions will necessarily occur over a range of crystallinities that will be controlled by both the specifics of the crystal population (size and shape distributions) and conditions of local stress. This pa-

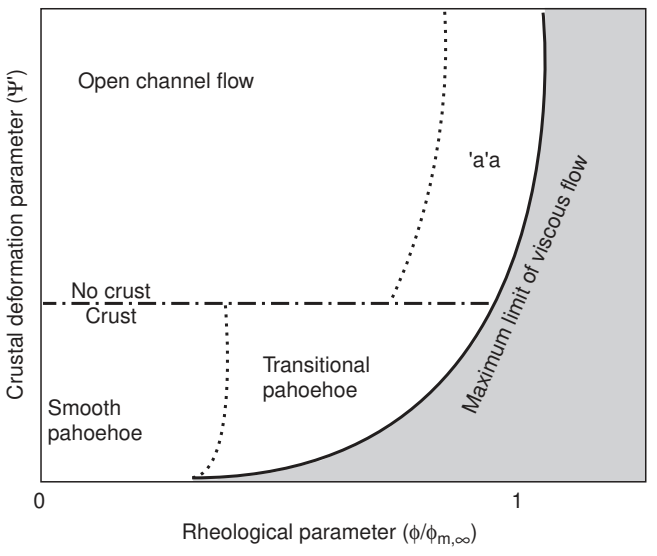

Fig. 11 Rheological and dynamic classification of basaltic lava flow morphologies. Both axes are dimensionless. Transitions in flow morphology are shown in the context of a crustal deformation parameter (here viewed as analogous to the Ψ parameter of Fink and Griffiths 1992; termed Ψ') and a rheological parameter (shown here as $\phi/\phi_{m,\infty}$). Ψ' determines conditions for stable crust formation (and thus pāhoehoe formation); $\phi/\phi_{m,\infty}$ determines the flow surface response to deformation and thus surface roughness. All boundaries are schematic but incorporate limited existing data that indicate flow transitions over a range of both crystallinity and strain rate

rameterization of basaltic lava facies transitions is equivalent to, but more specific than, the "thermal maturity" categorization of Naranjo et al. (1992).

Finally, we can use our observations to define conditions that lead to lava flow fields of predominantly pāhoehoe or ʻaʻā morphologies. We suggest that the dominant emplacement style is determined early in a flow's history and depends on the extent to which crust is permitted to form during early stages of flow. Early crust formation insulates flow interiors, allowing slow cooling by conductive heat transfer through the growing crust and promoting pāhoehoe flow field development. In contrast, continuous crustal disruption characteristic of open channel flows allows rapid, radiative cooling of flow interiors, consequent rapid crystallization (with nucleation aided by stirring), down-channel transitions to ʻaʻā, and flow interiors that behave as Bingham fluids. The latter condition will be promoted by high rates of effusion (e.g., Rowland and Walker 1990), steep slopes, and eruption of initially microlite-rich lava (e.g., through degassing-induced crystallization; Pinkerton and Sparks 1978; Lipman and Banks 1987).

Conclusion

The 16 May 1997 channelized ʻaʻā flow from Kīlauea cooled and crystallized rapidly over the first 2 km of transport away from the vent. Stirring of the flow resulted in continued crustal disruption and cooling throughout the entire flow thickness, as indicated by measured channel flow and overflow glass temperatures and crystallinities. A channel overflow $\sim$1 km from the vent had a crystallinity of 7% and developed a smooth pāhoehoe surface. Channel samples and breakouts from the medial channel had $\sim$15% crystallinity, and breakouts had transitional pāhoehoe morphologies. Textural measurements indicate that crystallization occurred through both crystal nucleation and growth, with nucleation predominating. Nucleation rates were high ($>10^4\,cm^{-3}s^{-1}$) and likely enhanced by energetic stirring of the flow.

Transformation to ʻaʻā surface morphology initiated along channel margins and occurred 1.9 km from the vent, where the channel had a uniform gradient, rather than 1.75 km from the vent, where lava flowed over a small lava falls. Thus, the transition was not triggered by an increase in either strain rate or imposed stress. The quenched ʻaʻā sample has a glass temperature of 1099 °C and a crystallinity of $\sim$45%. Both crystallinity and crystal number densities are similar to ʻaʻā samples from other active and solidified Hawaiian lava flows. This similarity suggests that maximum rates of cooling and crystallization are limited by rates of radiative cooling with near-perfect mixing. We emphasize that crystallinity plays a critical role in the pāhoehoe-ʻaʻā transition, a view essentially that suggested by Alexander (1859) and popular throughout the late nineteenth and early twentieth century. However, we link these early observations to more recent descriptions of the transition (Swanson 1973; Peterson and Tilling 1980; Kilburn 1981, 1990; Rowland and Walker 1987, 1990) by recognizing the importance of both rheological changes in the fluid (particularly the onset of yield strength generated by crystallinity increases during flow) and relative rates of crust formation and disruption (a strain rate threshold). This view of the transition, involving both crustal stability and rheological changes in the lava, links local requirements for the pāhoehoe-ʻaʻā transition to general conditions for pāhoehoe and ʻaʻā flow formation.

Acknowledgements The authors gratefully acknowledge the comments and suggestions of D. Peterson, E. Wolfe, C. Kilburn, and J. Crisp which greatly improved the manuscript. K.V.C. also thanks M. Manga, M. Saar, M. Folley, S. Hoover, and R. Griffiths for helpful discussions about suspension rheology. K.V.C. acknowledges NSF support for the work (EAR9508144), and all authors acknowledge support from the USGS Volcano Hazards Program.

References

Alexander WD (1859) Later details from the volcano on Hawaii. Pacific Commercial Advertiser, p. 2

Alexander WD (1886) The craters of Mokuaweoweo, on Mauna Loa. Nature 34:232–234

Aubele JC, Crumpler LS, Elston WE (1988) Vesicle zonation and vertical structure of basalt flows. J Volcanol Geotherm Res 35:349–374

Barnes HA, Hutton JF, Walters K (1989) An introduction to rheology. Amsterdam, Elsevier

Calvari S, Pinkerton H (1998) Formation of lava tubes and extensive flow field during the 1991–1993 eruption of Mount Etna. J Geophys Res 103:27291–27302

Calvari S, Cotelli M, Neri M, Pompilio M, Scribano V (1994) The 1991–1993 Etan eruption: chronology and lava flow-field evolution. Acta Vulcanol 4:1–14

Cashman KV (1993) Relationship between crystallization and cooling rate: insight from textural studies of dikes. Contrib Mineral Petrol 113:126–142

Cashman KV, Kauahikaua JP (1997) Reevaluation of vesicle distributions in basaltic lava flows. Geology 25:419–422

Cashman KV, Mangan MT, Newman S (1994) Surface degassing and modifications to vesicle size distributions in Kīlauea basalt. J Volcanol Geotherm Res 61:45–68

Chang GL (1930) A review of the aa-pāhoehoe question. Volcano Lett 294:1–3

Crisp J, Baloga S (1990) A model for lava flows with two thermal components. J Geophys Res 95:1255–1270

Crisp J, Baloga S (1994) Influence of crystallization and entrainment of cooler material on the emplacement of basaltic ʻaʻā lava flows. J Geophys Res 99:11819–11832

Crisp J, Cashman KV, Bonini JA, Hougen SB, Pieri D (1994) Crystallization history of the 1984 Mauna Loa flow. J Geophys Res 99:7177–7198

Daly RA (1911) The nature of volcanic action. Am Acad Arts Sci Proc 47:47–122

Dana JD (1849) Geology: United States Exploring Expedition. Putnam, New York

Dana JD (1888) History of the changes in Mauna Loa craters. Am J Sci 33:433–451

Dragoni M (1989) A dynamical model of lava cooling by radiation. Bull Volcanol 51:88–95

Dragoni M (1993) Modelling the rheology and cooling of lava flows. In: Kilburn CRJ (ed) Active lavas. UCL Press, London, pp 235–261

Dragoni M, Tallarico A (1994) The effect of crystallization on the rheology and dynamics of lava flows. J Volcanol Geotherm Res 59:241–252

Dutton CE (1884) The Hawaiian volcanoes. US Geol Surv 4th Ann Rep, Government Printing Office, Washington DC, pp 75–219

Emerson OH (1926) The formation of aa and pahoehoe. Am J Sci 12:1–9

Finch RH (1926) The formation of aa and pahoehoe lava. Volcano Lett 86:1

Fink JH, Griffiths RW (1990) Radial spreading of viscous-gravity currents with solidifying crust. J Fluid Mech 221:485–509

Fink JH, Griffiths RW (1992) A laboratory study of the morphology of lava flows extruded from point and line sources. J Volcanol Geotherm Res 54:19–32

Fink JH, Grifiths RW (1998) Morphology, eruption rates, and rheology of lava domes: insights from laboratory models. J Geophys Res 103:527–546

Fink JH, Zimbelman JR (1986) Rheology of the 1983 Royal Gardens basalt flows, Kīlauea Volcano, Hawaii. Bull Volcanol 48:87–96

Fink JH, Zimbelman JR (1990) Longitudinal variations in rheological properties of lavas: Pu Oo Basalt Flows, Kīlauea Volcano, Hawaii. In: Fink JH (ed) Lava flows and domes. Springer, Berlin Heidelberg New York, pp 157–173

Gemmellaro C (1858) La vulcanologia dell'Etna. Accad Gioenia, Catania

Greeley R (1987) The role of lava tubes in Hawaiian volcanoes. US Geol Surv Prof Pap 1350:1589–1602

Gregg TKP, Fink JH (1995) Quantification of submarine lava-flow morphology through analog experiments. Geology 23:73–76

Griffiths RW, Fink JH (1992a) The morphology of lava flows in planetary environments: predictions from analog experiments. J Geophys Res 97:19739–19748

Griffiths RW, Fink JH (1992b) Solidification and morphology of submarine lavas: a dependence on extrusion rate. J Geophys Res 97:19729–19737

Griffiths RW, Fink JH (1993) Effects of surface cooling on the spreading of lava flows and domes. J Fluid Mech 252:667–702

Griffiths RW, Fink JH (1997) Solidifying Bingham extrusions: a model for the growth of silicic lava domes. J Fluid Mech 347:13–36

Guest JE, Kilburn CRJ, Pinkerton H, Duncan AM (1987) The evolution of lava flow-fields: observations of the 1981 and 1993 eruptions of Mount Etna, Sicily. Bull Volcanol 49:527–540

Hallot E, Davy P, D'Ars J de B, Auvray B, Martin H, Van Damme H (1996) Non-Newtonian effects during injection in partially crystallized magmas. J Volcanol Geotherm Res 71:31–44

Heliker CC, Mangan MT, Mattox TN, Kauahikaua JP, Helz RT (1998) The character of long-term eruptions: inferences from episodes 50–53 of the Pu'u 'Ō'ō Kūpaianaha eruption of Kīlauea Volcano. Bull Volcanol 59:381–393

Helz RT, Thornber CR (1987) Geothermometry of Kīlauea Iki lava lake. Bull Volcanol 49:651–658

Helz RT, Heliker CC, Mangan MT, Hon K, Neal CA, Simmons L (1991) Thermal history of current Kīlauean East Rift eruption. Eos 72:557–558

Helz RT, Banks NG, Heliker CC, Neal CA., Wolfe EW (1995) Comparative geothermometry and thermal history of recent Hawaiian eruptions. J Geophys Res 100:17637–17657

Higgins M (1994) Numerical modeling of crystal shapes in thin sections: estimation of crystal habit and true size. Am Mineral 79:113–119

Hon K, Kauahikaua JP, Denlinger R, Mackay K (1994) Emplacement and inflation of pāhoehoe sheet flows: observations and measurements of active lava flows on Kīlauea, Hawai'i. Geol Soc Am Bull 106:351–370

Hulme G (1974) The interpretation of lava flow morphology. J Geophys Res 39:361–383

Jaggar TA (1920) Seismometric investigation of the Hawaiian lava column. Bull Seismol Soc Am 10:155–275

Jaggar TA (1930) Distinction between pahoehoe and aa or block lava. Volcano Lett 281:1–4

Jurado-Chichay Z, Rowland SK (1995) Channel overflows of the Pohue Bay flow, Mauna Loa, Hawaii: examples of the contrast between surface and interior lava. Bull Volcanol 57:117–126

Katz MG (1997) Patterns of lava flow coverage in drill cores. Thesis, Univ Oregon

Kauahikaua JP, Cashman KV, Mattox TN, Hon K, Heliker CC, Mangan MT, Thornber CR (1998) Observations on basaltic lava streams in tubes from Kīlauea Volcano, Hawai'i. J Geophys Res 103:27303–27324

Kerr RC, Lister JR (1991) The effects of shape on crystal settling and on the rheology of magmas. J Geol 99:457–467

Keszthelyi L (1995) A preliminary thermal budget for lava tubes on the Earth and Planets. J Geophys Res 100:20411–20420

Kilburn CRJ (1981) Pahoehoe and aa lavas: a discussion and continuation of the model of Peterson and Tilling. J Volcanol Geotherm Res 11:373–389

Kilburn CRJ (1990) Surfaces of aa flow-fields on Mount Etna, Sicily: morphology, rheology, crystallization and scaling phenomena. In: Fink J (ed) Lava flows and domes. Springer, Berlin Heidelberg New York, pp 129–156

Kilburn CRJ (1993) Lava crusts, aa flow lengthening and the pāhoehoe-'a'ā transition. In: Kilburn CRJ (ed) Active lavas. UCL Press, London, pp 263–280

Kilburn CRJ (1996) Patterns and predictability in the emplacement of subaerial lava flows and flow fields. In: Scarpa C, Tilling R (eds) Monitoring and mitigation of volcano hazards. Springer, Berlin Heidelberg New York, pp 491–537

Kilburn CRJ, Guest JE (1993) aa lavas of Mount Etna, Sicily. In: Kilburn CRJ (ed) Active lavas. UCL Press, London, pp 73–106

Kouchi A, Tsuchiyama A, Sunagawa I (1986) Effect of stirring on crystallization kinetics of basalt: texture and element partitioning. Contrib Mineral Petrol 93:429–438

Krieger IM, Dougherty TJ (1959) A mechanism for non-Newtonian flow in suspensions of rigid spheres. Trans Soc Rheol 3:137–152

Lejeune A-M, Richet P (1995) Rheology of crystal-bearing silicate melts: an experimental study at high viscosities. J Geophys Res 100:4215–4230

Lesher CE, Cashman KV, Mayfield JD (in press) Kinetic controls on the crystallization of Tertiary North Atlantic basalts: implications for the emplacement and cooling histories of near-vent lavas at ODP Site 989, SE Greenland rifted margin. ODP Sci Res Leg 163

Lipman PW, Banks NG (1987) Aa flow dynamics, Mauna Loa, 1984. US Geol Surv Prof Pap 1350:1527–1567

Lofgren GE (1980) Experimental studies on the dynamic crystallization of silicate melts. In: Hargraves RB (ed) Physics of magmatic processes. Princeton University Press, Princeton, pp 487–551

Macdonald GA (1953) Pahoehoe, aa, and block lava. Am J Sci 251:169–191

Mangan MT, Heliker CC, Mattox TN, Kauahikaua JP, Helz RT (1995) Episode 49 of the Pu'u 'Ō'ō Kūpaianaha eruption of Kīlauea Volcano: breakdown of a steady-state eruptive era. Bull Volcanol 57:127–135

Marsh BD (1981) On the crystallinity, probability of occurrence, and rheology of lava and magma. Contrib Mineral Petrol 78:85–98

Miyamoto H, Sasaki S (1998) Numerical simulations of flood basalt lava flows: roles of parameters on lava flow morphologies. J Geophys Res 103:27489–27502

Montierth C, Cashman KV (1996) A textural and experimental study of the paired pāhoehoe and aa flows of 1859, Mauna Loa Volcano, Hawaii. Geol Soc Am (abstr with programs) 28:93

Montierth CM, Johnston AD, Cashman KV (1995) An empirical composition-based glass geothermometer for Mauna Loa lava. Geophys Monogr 92:207–217
Moore HJ (1987) Preliminary estimates of the rheological properties of 1984 Mauna Loa lava. US Geol Surv Prof Pap 1350:1569–1588
Mullin JW (1976) Industrial crystallization. Plenum Press, New York
Naranjo JA, Sparks RSJ, Stasiuk M, Moreno H, Ablay GJ (1992) Morphological, structural and textural variations in the 1988–1990 andesite lava of Lonquinmay Volcano, Chile. Geol Mag 129:657–678
Neal CA, Duggan TJ, Wolfe EW, Brandt EL (1988) Lava samples, temperatures, and compositions. US Geol Surv Prof Pap 1463:99–126
Oleson WB (1880) On the Mauna Loa lava flow of 1880. Hawaiian Gazette, p 3
Pareschi MT, Pompilio M, Innocenti F (1990) Automated evaluation of volumetric grain-size distribution from thin-section images. Comp Geosci 16:1067–1084
Peterson DW, Swanson DA (1974) Observed formation of lava tubes. Stud Speleol 2:209–222
Peterson DW, Tilling RI (1980) Transition of basaltic lava from pahoehoe to aa, Kilauea Volcano, Hawaii: field observations and key factors. J Volcanol Geotherm Res 7:271–293
Peterson DW, Holcomb RT, Tilling RI, Christiansen RL (1994) Development of lava tubes in the light of observations at Mauna Ulu, Kīlauea Volcano, Hawai'i. Bull Volcanol 56:343–360
Peterson T (1996) A refined technique for measuring crystal size distributions in thin section. Contrib Mineral Petrol 124:395–405
Philpotts AR, Shi J, Brustman C (1998) Role of plagioclase crystal chains in the differentiation of partly crystallized basaltic magma. Nature 395:343–346
Pinkerton H, Norton G (1995) Rheological properties of basaltic lavas at sub-liquidus temperatures: laboratory and field measurements on lavas from Mount Etna. J Volcanol Geotherm Res 68:307–323
Pinkerton H, Sparks RSJ (1976) The 1975 sub-terminal lavas, Mount Etna: a case history of the formation of a compound lava field. J Volcanol Geotherm Res 1:167–182
Pinkerton H, Sparks RSJ (1978) Field measurements of the rheology of flowing lava. Nature 276:383–385
Pinkerton H, Stevenson RJ (1992) Methods of determining the rheological properies of magmas at sub-liquidus temperatures. J Volcanol Geotherm Res 53:47–66
Pinkerton H, Wilson L (1994) Factors controlling the lengths of channel-fed lava flows. Bull Volcanol 56:108–120
Polacci M, Papale P (1997) The evolution of lava flows from ephemeral vents at Mount Etna: insights from vesicle distribution and morphological studies. J Volcanol Geotherm Res 76:1–17
Polacci M, Cashman KV, Kauahikaua JP (1999) Textural characterization of the pāhoehoe-'a'ā transition in Hawaiian basalt. Bull Volcanol 60:595–609
Probstein RF, Sengun MZ, Tseng T-C (1994) Bimodal model of concentrated suspension viscosity for distributed particle sizes. Rheol Acta 38:811–829
Robson GR (1967) Thickness of Etnean lavas. Nature 216:251–252
Rowland SK, Walker GPL (1987) Toothpaste lava: characteristics and origin of a lava structural type transitional between pahoehoe and aa. Bull Volcanol 49:631–641
Rowland SK, Walker GPL (1990) Pahoehoe and aa in Hawaii: volumetric flow rate controls the lava structure. Bull Volcanol 52:631–641
Ryerson FJ, Weed HC, Piwinskii AJ (1988). Rheology of subliquidus magmas I. Picritic compositions. J Geophys Res 93:3421–3436
Sahagian DL, Proussevitch AA (1998) 3D particle size distributions from 2D observations: stereology for natural applications. J Volcanol Geotherm Res 84:173–196
Sato H (1995) Textural difference between pahoehoe and aa lavas of Izu-Oshima volcano, Japan: an experimental study on population density of plagioclase. J Volcanol Geotherm Res 66:101–113
Scrope GP (1856) On the formation of craters, and the nature of the liquidity of lavas. Q J Geol Soc Lond 12:326–350
Shaw HR, Wright TL, Peck DL, Okamura R (1968) The viscosity of basaltic magma: analysis of field measurements of Makaophui lava lake. Am J Sci 226:225–264
Shaw HR (1969) Rheology of basalt in the melting range. J Petrol 10:510–535
Smith JV (1997) Shear thickening dilatency in crystal-rich flows. J Volcanol Geotherm Res 79:1–8
Sparks RSJ, Pinkerton H (1978) Effect of degassing on rheology of basaltic lava. Nature 276:385–386
Stearns HT, Clark WO (1930) Geology and water resources of the Kau district, Hawai'i. US Geol Surv Water-Supply Pap 616:1–194
Swanson DA (1973) Pahoehoe flows from the 1969–1971 Mauna Ulu eruption, Kilauea Volcano, Hawaii. Geol Soc Am Bull 84:615–626
Thornber CR, Heliker CC, Reynolds JR, Kauahikaua JP, Okubo P, Lisowski M, Sutton J, Clague D (1996) The eruptive surge of February 1, 1996:a highlight of Kīlauea's ongoing east rift zone eruption. Eos 77:798
Thornber CR, Sherrod D, Heliker CC, Kauahikaua JP, Trusdell F, Lisowski M, Okubo P (1997) Kīlauea's ongoing eruption: Napau Crater revisited after 14 years. Eos 78:329
Uhlmann DR, Onorato PIK, Scherer GW (1979) A simplified model for glass formation. Tenth Proc Lunar Planet Sci Conf, pp 375–381
Underwood EE (1970) Quantitative stereology. Addison-Wesley, Reading, Mass.
Walker GPL (1967) Thickness and viscosity of Etnean lavas. Nature 213:484–485
Walker GPL (1989) Spongy pahoehoe in Hawaii: a study of vesicle-distribution patterns in basalt and their significance. Bull Volcanol 51:199–209
Washington HS (1923) Petrology of the Hawaiian Islands IV. The formation of aa and pahoehoe. Am J Sci 6:409–423
Wildemuth CR, Williams MC (1984) Viscosity of suspensions modeled with a shear-dependent maximum packing fraction. Rheol Acta 23:627–635
Wildemuth CR, Williams MC (1985) A new interpretation of viscosity and yield stress in dense slurries: coal and other irregular particles. Rheol Acta 24:75–91
Wolfe EW, Neal CA, Banks NG, Duggan TJ (1988) Geologic observations and chronology of eruptive events. In: Wolfe EW (ed) The Puu Oo eruption of Kīlauea Volcano, Hawaii: episodes 1 through 20, January 3, 1983 through June 8, 1984. US Geol Surv Prof Pap 1453:1–99
Wright TL, Okamura RT (1977) Cooling and crystallization of tholeiitic basalt, 1965 Makaopuhi lava lake, Hawaii. US Geol Surv Prof Pap 1004:1–78
Wright TL, Takahashi TJ (1989) Observations and interpretation of Hawaiian volcanism and seismicity 1779–1955:an annotated bibliography and subject index. University of Hawaii Press, Honolulu, Hawaii
Wright TL, Takahashi TJ (1998) Hawaii bibliographic database. Bull Volcanol 59:276–280
Zhou JZQ, Fang T, Luo G, Uhlherr PHT (1995) Yield stress and maximum packing fraction of concentrated suspensions. Rheol Acta 34:544–561